Human Molecular Genetics, 2007, Vol. 16, No. 4 **431–444**
doi:10.1093/hmg/ddl477
Advance Access published on January 8, 2007

Increased longevity and refractoriness to Ca^{2+}-dependent neurodegeneration in Surf1 *knockout* mice

Carlotta Dell'Agnello[1,†], Sara Leo[2,†], Alessandro Agostino[1], György Szabadkai[2,‡], Cecilia Tiveron[3], Alessandra Zulian[1], Alessandro Prelle[4], Pierre Roubertoux[5], Rosario Rizzuto[2] and Massimo Zeviani[1,*]

[1]Unit of Molecular Neurogenetics, Pierfranco and Luisa Mariani Center for the Study of Children's Mitochondrial Disorders, National Neurological Institute 'C. Besta', Milano, Italy, [2]Department of Experimental and Diagnostic Medicine, Section of General Pathology, Interdisciplinary Center for the Study of Inflammation (ICSI) and ER-GenTech, University of Ferrara, Ferrara, Italy, [3]Foundation EBRI Rita Levi-Montalcini Disease Modelling Facility, Rome, Italy, [4]Centro Dino Ferrari, UO Neurologia, Fondazione Ospedale Maggiore Policlinico, Mangiagalli e Regina Elena, IRCCS, Milano and [5]Université Marseille-2, CNRS-Université de la Méditerranée, Marseille, France

Received November 3, 2006; Revised December 19, 2006; Accepted December 28, 2006

Leigh syndrome associated with cytochrome c oxidase (COX) deficiency is a mitochondrial disorder usually caused by mutations of *SURF1*, a gene encoding a putative COX assembly factor. We present here a *Surf1*−/− recombinant mouse obtained by inserting a *loxP* sequence in the open reading frame of the gene. The frequency of −/−, +/+ and +/− genotypes in newborn mice followed a mendelian distribution, indicating that the ablation of Surf1 is compatible with postnatal survival. The biochemical and assembly COX defect was present in *Surf1*^{loxP}−/− mice, but milder than in humans. Surprisingly, not only these animals failed to show spontaneous neurodegeneration at any age, but they also displayed markedly prolonged lifespan, and complete protection from Ca^{2+}-dependent neurotoxicity induced by kainic acid. Experiments on primary neuronal cultures showed markedly reduced rise of cytosolic and mitochondrial Ca^{2+} in *Surf1*^{loxP}−/− neurons, and reduced mortality, compared to controls. The mitochondrial membrane potential was unchanged in KO versus wild-type neurons, suggesting that the effects of the ablation of Surf1 on Ca^{2+} homeostasis, and possibly on longevity, may be independent, at least in part, from those on COX assembly and mitochondrial bioenergetics.

INTRODUCTION

Cytochrome c oxidase (COX), the terminal enzyme of the mitochondrial respiratory chain (MRC), catalyzes the transfer of electrons from reduced cytochrome c to molecular oxygen (1). COX is composed of 13 protein subunits, the three largest being encoded by mtDNA genes, and the remaining ten are encoded by nuclear DNA genes (2). A number of accessory factors are necessary for the formation of an active holoenzyme complex (3), including those involved in synthesis of heme a, incorporation of copper atoms and assembly of the protein backbone (4). One of these factors, SURF1, is a 30 kDa hydrophobic protein embedded in the inner membrane of mitochondria. The absence, or malfunctioning, of SURF1p determines the accumulation of COX assembly intermediates, and a drastic reduction in the amount of fully assembled enzyme, in both yeast (5) and humans (6). As a consequence, profound COX deficiency (7) in multiple tissues of Surf1

*Correspondence should be addressed to: Via L. Temolo 4, 20126 Milano, Italy. Tel: +33 390223942630; Fax: +33 390223942619; Email: zeviani@fastwebnet.it
†These authors contributed equally to the work.
‡Present address: INSERM U807, University Paris 5, Faculty of Medicine Necker-Enfants Malades, Paris, France.

mutant patients (8) leads to the development of Leigh syndrome (LS^{COX}), an early onset, invariably fatal mitochondrial encephalomyelopathy (9).

In vertebrates, *SURF1* is part of the very tight and highly conserved *surfeit* gene cluster, which includes six genes (*SURF1–6*) (10). The reason for long-standing maintenance of such a compact physical organization is obscure, since the corresponding SURF proteins are neither functionally nor structurally related to each other. The precise function of the *SURF1* gene product itself remains unknown, although the results of several studies in yeast and mammals suggest a role for SURF1 protein (SURF1p) as an auxiliary chaperone-like factor, involved in the early assembly steps of the COX protein backbone (6).

To better understand the role of SURF1p and the pathogenesis of LS^{COX}, we have previously created a constitutive *knockout* (KO) mouse model, in which exons 5–7 of the *Surf1* gene were replaced by a neomycin-resistance (*NEO*) cassette (11). Approximately 90% of the $Surf1^{NEO}-/-$ mice died at E6.5–7.5. The few animals that reached birth partially recapitulated, although to a lesser extent, the biochemical findings, but failed to display the clinical and neuro-pathological features of human LS^{COX}.

We present here a second *Surf1* KO model, based on the insertion of a *loxP* sequence in exon 7 of the murine *Surf1* gene ($Surf1^{loxP}$), leading to an aberrant, prematurely truncated and highly unstable protein. The +/+, +/− and −/− genotypes in newborn animals were in agreement with the mendelian distribution, indicating that, rather than to the ablation of *Surf1* itself, the high embryonic lethality observed in the previous $Surf1^{NEO}-/-$ model was due to a spurious effect of the *NEO* cassette on the expression of neighboring genes. Similar to the previous $Surf1^{NEO}-/-$ mice, the $Surf1^{loxP}-/-$ mice displayed mild reduction of COX activity in all tissues, but no lesion resembling LS^{COX} encephalopathy was ever observed. However, when the sensitivity to Ca^{2+}-dependent excitotoxicity was tested in both $Surf1^{loxP}-/-$ brains and neuronal cell cultures, we observed a virtually complete protection from *in vivo* neurodegeneration induced by exposure to high doses of kainic acid, a glutamatergic epileptogenic agonist. In addition, $Surf1^{loxP}-/-$ mice showed a marked increase in longevity, compared to heterozygous or homozygous wild-type (*wt*) littermates. These data suggest a role for Surf1p in intracellular Ca^{2+} homeostasis and mitochondrial control of aging.

RESULTS

Generation of $Surf1^{loxP}-/-$ mice

The strategy used to disrupt the mouse *Surf1* gene (NM_013677) is shown in Figure 1A. Briefly, a cDNA expressing the *Escherichea coli* neomycin phosphotransferase (NEO), therefore conferring neomycin-resistance, flanked by two *loxP* sequences (*loxP-NEO-loxP* cassette), was inserted into a unique *Acc*III restriction site of *Surf1* exon 7. In order to confirm homologous recombination, Southern blot analysis was performed on both extremities of the $Surf1^{loxP\text{-}NEO\text{-}loxP}$ recombinant allele (Fig. 1B and C). Blastocyst injection of two recombinant clones gave rise to eleven $Surf1^{loxP\text{-}NEO\text{-}loxP}$ chimeric mice showing germline transmission. No $Surf1^{loxP\text{-}NEO\text{-}loxP/loxP\text{-}NEO\text{-}loxP}$ homozygous individuals were obtained by mating $Surf1^{loxP\text{-}NEO\text{-}loxP/+}$ heterozygotes to each other, due to arrest of organogenesis at E8.5–9.5 (Supplementary Materials, Fig. 1 and Table 1). The *NEO* cassette and one of the two *loxP* sequences were then excised by mating $Surf1^{loxP\text{-}NEO\text{-}loxP/+}$ heterozygous animals with animals constitutively expressing the *cre* recombinase. The resulting recombinant allele ($Surf1^{loxP}$) contains a single *loxP* insertion (Fig. 1D), which causes the shift of the open reading frame (ORF) from nt 674 downstream of the mouse *Surf1* cDNA, and the replacement of the codon encoding N_{225} into a TAA stop codon (N225X) (Fig. 1A). This mutation predicts the elimination of 81 amino acids on the Surf1p carboxy terminus. No cross-reacting material was detected by western blot immunoassay using polyclonal and monoclonal anti-Surf1 antibodies in several tissues of our $Surf1^{loxP}-/-$ mice (Fig. 1F), indicating that the truncated $Surf1^{loxP}$ protein is either unstable or fails to be translated, due to mRNA decay (Fig. 1E).

Clinical and biochemical phenotype

The percentages of approximately 800 $Surf1^{loxP}-/-$, +/− and +/+ newborn animals followed a mendelian distribution (26, 51 and 23%, respectively; Supplementary Material, Fig. 2A). Newborn $Surf1^{loxP}-/-$ individuals were significantly smaller than their littermates, but this difference progressively disappeared after weaning (Supplementary Material, Fig. 2B). No difference in the clinical phenotype was observed between $Surf1^{loxP}-/-$ individuals and their +/− or +/+ littermates, including the appearance of neurological symptoms, abnormal reaction to stimuli, aberrant behavior, impaired cognitive abilities and reduced fertility. There was a small but significant reduction at the rotarod test (Supplementary Material, Fig. 2C), indicating mildly decreased motor skills in $Surf1^{loxP}-/-$ versus *wt* mice.

Histochemically, we observed decreased reaction to COX and increased reaction to succinate dehydrogenase (SDH) in $Surf1^{loxP}-/-$ skeletal muscle (Fig. 2A), similar to, but less severe than, that observed in *SURF1* mutant patients. Finally, $Surf1^{loxP}-/-$ brains showed normal cytoarchitecture by thionine and GFAP stainings (data not shown).

Biochemically, there was no difference in the activities of MRC complexes I, II and III, whereas the COX activity in several tissues of $Surf1^{loxP}-/-$ individuals was 30–50% that of control littermates (Fig. 2B). Again, this reduction was much less marked than that observed in LS^{COX} patients (7). $Surf1^{loxP}+/-$ mice showed no biochemical difference compared to *Surf1* +/+ littermates, as expected for a recessive trait (data not shown).

Blood lactate was higher in $Surf1^{loxP}-/-$ mice than in *wt* littermates, indicating partial block in the aerobic utilization of pyruvate (Supplementary Material, Fig. 2D).

As exemplified in Fig. 2C, fully assembled COX was variably reduced in different tissues of $Surf1^{loxP}-/-$ mice, to an extent compatible with the levels of residual COX activity. Early assembly COX intermediates were also present in isolated mitochondria of $Surf1^{loxP}-/-$ mice, similar to, but much lesser than, what is found in *SURF1* mutant patients.

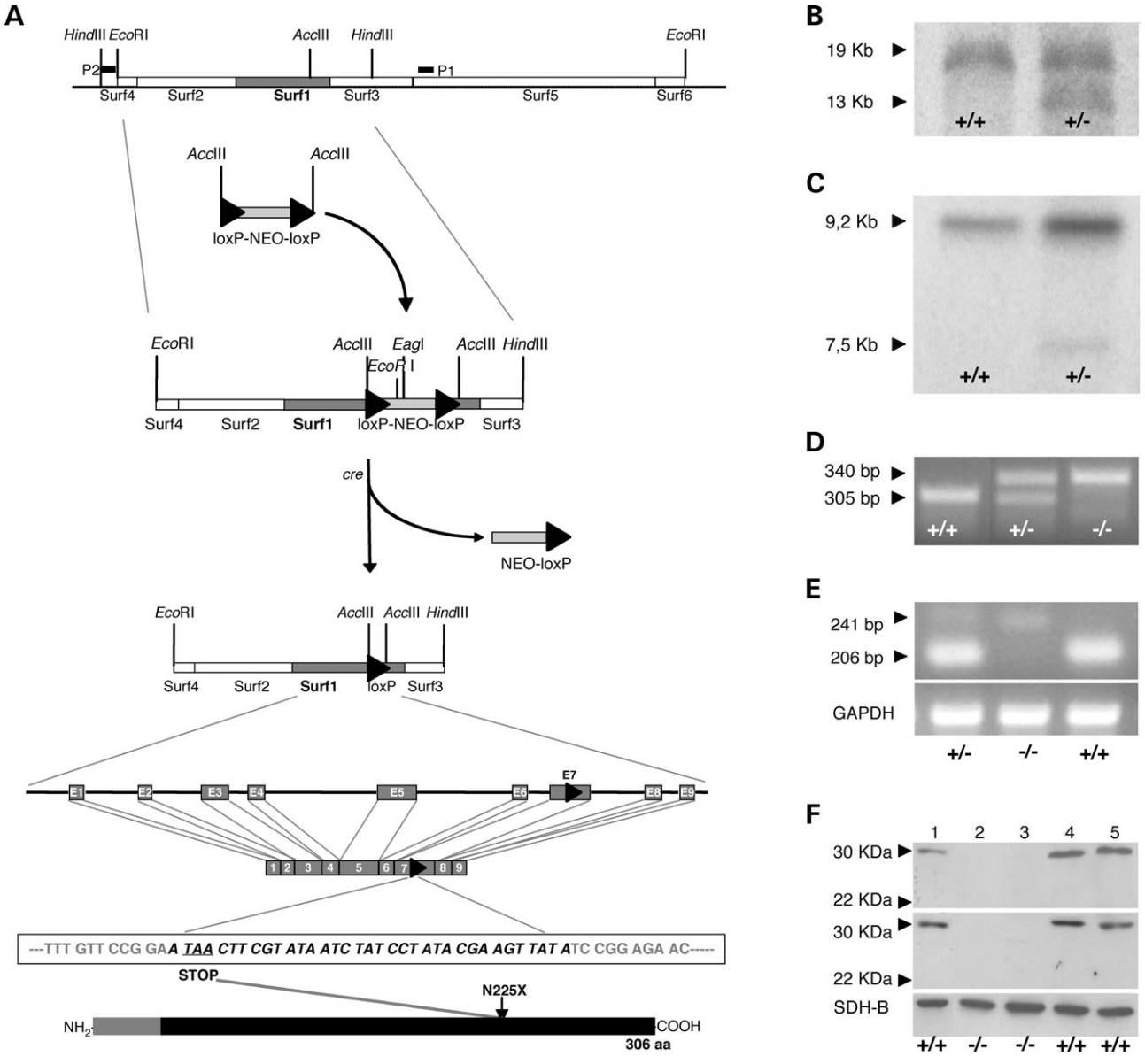

Figure 1. Generation of Surf1−/− mice (see Materials and Methods). (**A**) Schematic representation of the *Surf1* locus, $Surf1^{loxP\text{-}NEO\text{-}loxP}$ and $Surf1^{loxP}$ alleles, $Surf1^{loxP}$ cDNA and $Surf1^{loxP}$ proteins. P1 and P2 refer to the probes used for Southern-blot analysis shown in panels **B** and **C**. Numbers in the scheme of the *Surf1* gene and *Surf1* cDNA refer to exons 'E'. In the nucleotide sequence of the $Surf1^{loxP}$ allele, exon 7 is in gray, the *loxP* sequence is in black and italicized, the TAA stop codon is underlined. In the scheme of the Surf1 protein (bottom part of panel A), the putative mitochondrial targeting peptide is in gray. (B and C) Southern-blot analysis of the recombinant $Surf1^{loxP\text{-}NEO\text{-}loxP}$ allele. (**D**) PCR-based genotyping of the $Surf^{loxP}$ versus $Surf^{wt}$ alleles. (**E**) RT-PCR analysis of the $Surf^{loxP}$ versus $Surf^{wt}$ alleles. The *GAPDH* cDNA fragment serves as a control. (**F**) Western blot analysis. Surf1p cross-reacting material is absent in mitochondrial membranes isolated from different $Surf^{loxP}-/-$ organs probed with a monoclonal anti-Surf1p antibody (upper panel) and with a polyclonal antibody against the Surf1p mid portion (middle panel). The 30 kDa SDH-B subunit was used as a loading control (bottom panel). Lane 1, control fibroblasts; lanes 2 and 4, brain; lanes 3 and 5, liver.

Taken together, these data are remarkably similar to those previously reported for the surviving $Surf1^{NEO}-/-$ individuals (11).

Increased longevity of $Surf1^{loxP}-/-$ mice

In order to evaluate whether the lack of Surf1p could determine a late-onset phenotype, $Surf1^{loxP}-/-$ mice and control littermates were maintained under continuous observation in the same standard breeding conditions. No neurological or other clinical symptoms were ever seen in any individual. However, the lifespan was markedly different between the two groups. A total of 25/43 $Surf1^{loxP}-/-$ mice died during the observation period, against 30/48 deaths recorded in the control group. The median survival was 793 days for the $Surf1^{loxP}-/-$ group and 654 days for the control group, the latter being the standard median survival reported for laboratory mice (12). As shown in Figure 3A, the difference in the Kaplan–Meier survival

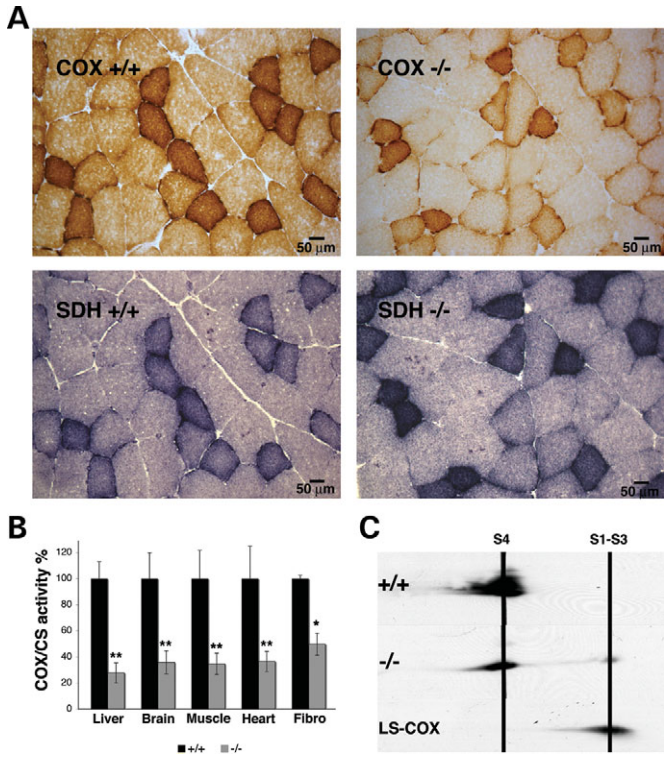

Figure 2. Histochemical and biochemical characterization of *Surf1*^{loxP} mice. (**A**) Serial sections of the left quadriceps from 5-month-old *Surf1*$^{loxP}-/-$ versus *Surf1* $+/+$ animals. Several fibers in the *Surf1*$^{loxP}-/-$ muscle show reduced reaction to COX and are hyper-intense to SDH, compared to the *Surf1* $+/+$ muscle. (**B**) COX/CS activities of 3-month-old *Surf1*$^{loxP}-/-$ mice ($n = 10$) compared to *Surf1*$+/+$ littermates ($n = 10$) taken as 100%. $^{*}P < 0.01$; $^{**}P < 10^{-5}$. (**C**) Western blot analysis of 2D-BNE on isolated mitochondria from $-/-$ and $+/+$ livers and from fibroblasts of a SURF1 mutant patient (LS-COX), using an anti-COXI antibody. S4 indicates mature, fully assembled COX; S1–S3 indicate early assembly intermediates.

probability, calculated by the logrank test, was highly significant between the two groups ($P = 0.0002$), irrespective of the gender (Fig. 3B and C).

Surf1$^{loxP}-/-$ mice are protected from Ca^{2+}-related excitotoxic brain damage

In order to determine whether our *Surf1*$^{loxP}-/-$ mice were more susceptible to stress-induced neuronal damage, we used kainic acid, an epileptogenic glutamate agonist that has extensively been used to test neuronal response and survival to Ca^{2+}-mediated excitotoxicity. We injected *intra peritoneum* (*i.p.*) a total of 145 three-month old mice (73 controls and 72 *Surf1*$^{loxP}-/-$) with 30 mg/kg of kainic acid. The mortality rate, as well as the frequency, time lapse, severity and duration of the kainate-induced seizures were similar between the KO and control groups (Table 1), suggesting that the pharmacokinetics of the drug did not differ in the two groups. Following a standard protocol (13), only animals surviving the most severe level-5 seizure were further investigated (Table 1). Whole-brain pathological examination was carried out using the neurodegeneration-sensitive FluoroJadeB (FJB) fluorochrome (14) and thionine stainings. Strong FJB-positive neurons

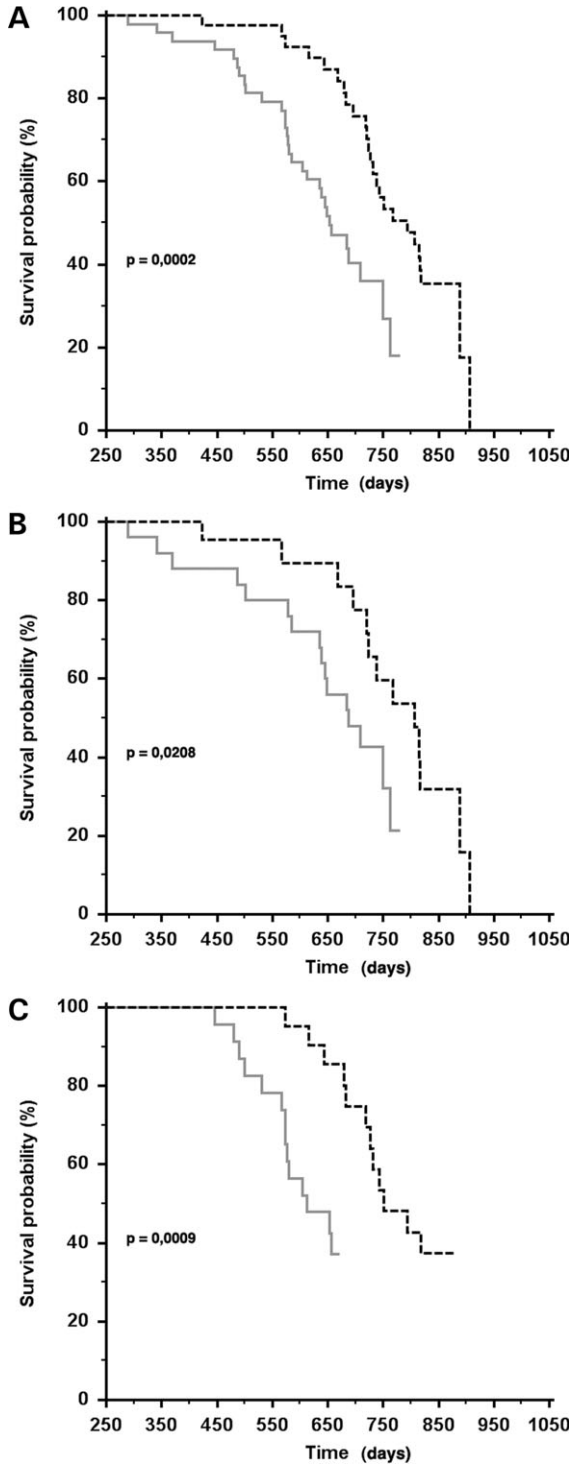

Figure 3. Kaplan–Meier survival analysis on *Surf1*$^{loxP}-/-$ (dotted black curves, $n = 43$) versus *Surf1*$+/+$ (gray lines, $n = 48$) mice. (**A**) Total. (**B**) Females ($n = 22 + 25$). (**C**) Males ($n = 21 + 23$). Significance (P) was calculated by the logrank test.

were detected in virtually all the glutamatergic areas of the control brains, including the *Cornu Ammonis* (CA) areas 1–4 of the *hippocampus*, the cerebral cortex, the amygdala and the thalamic and olfactory nuclei. The most severely

Table 1. Kainic acid treatment

	+/+	−/−
Injected animals	73	72
Death during crisis	13	12
Total L5[a] mice analyzed	24	23
Analyzed after 1 day	11	11
2 days	4	3
4 days	3	2
9 days	2	2
60 days	4	5

[a]L5, level-5 seizures (13).

affected areas were the CA1 and CA3 regions, which stained consistently FJB-positive in all of the 24 control mice. Other brain areas were differently affected in different *wt* animals. However, no FJB-positive cells were ever detected in all of the 23 *Surf1*^{loxP}−/− brains (Fig. 4). Differential uptake of kainic acid by *Surf1*^{loxP}−/− versus control neurons was unlikely, since there was no appreciable difference in the amount of glutamate ionotropic receptor subunits, immunovisualized using specific antibodies (Supplementary Material, Fig. 3). As exemplified in Fig. 5, severe neuronal loss in glutamatergic areas was observed in kainate-treated *wt* brains stained with thionine, while *Surf1*^{loxP}−/− brains appeared consistently identical to untreated control brains. TUNEL-positive apoptotic nuclei were abundant in CA1–4 neurons (Fig. 5G–I) and in neurons from other glutamatergic regions of treated *wt* brains (data not shown). No TUNEL-positive neurons were ever detected in the same regions of *Surf1*^{loxP}−/− brains.

Glutamate-induced cytosolic Ca^{2+} signals and consequent neuronal cell death are reduced in *Surf1*^{loxP} −/− neurons

Kainic acid treatment mimics glutamate-induced excitotoxicity, which is characterized by delayed Ca^{2+} deregulation (DCD) and loss of mitochondrial potential ($\Delta\Psi_m$) (15,16). Glutamate stimulation leads to the activation of metabotropic (mGlu) and ionotropic (AMPA, kainate and NMDA-type) plasma-membrane receptors in neurons. To further investigate the impact of *Surf1* ablation on these phenomena, we used 7-day-old cortical/hippocampal primary neuronal cell cultures obtained from *Surf1*^{loxP}−/− mice and controls. Activation of the metabotropic receptor leads to inositol-triphosphate (IP_3)-induced Ca^{2+} release from the endoplasmic reticulum (ER). Metabotropic Ca^{2+} responses were not detected in cultured neuronal cells, as confirmed by the use of the specific mGlu agonist APB (data not shown). Activation of ionotropic receptors causes Na^+-mediated cell depolarization and subsequent Ca^{2+} influx through voltage-dependent Ca^{2+} channels, as well as direct Ca^{2+} influx through activation of the NMDA channel. To measure cytosolic Ca^{2+} signals, we loaded neurons with the low-affinity Ca^{2+} dye fura-FF. Neurons were then challenged with 10 or 100 μM glutamate for 30 min, and cytosolic [Ca^{2+}] ([Ca^{2+}]$_c$) changes were measured in single cells. As shown in Figure 6A and B, the increase in [Ca^{2+}]$_c$ induced by 10 μM glutamate was not significantly different in *Surf1*^{loxP}−/− versus *Surf1*+/+ neurons (ΔF/F 0.10 ± 0.01 in *Surf1*^{loxP}−/− versus 0.12 ± 0.01 in *Surf1*+/+, $n > 100$ for each group, $P = 0.31$), but it was much lower after exposure to 100 μM glutamate (ΔF/F = 0.26 ± 0.02 in *Surf1*^{loxP}−/− versus 0.45 ± 0.03 in *Surf1*+/+, $n > 140$ for each group, $P < 10^{-5}$).

Sustained stimulation with high doses of glutamate induces deregulation of neuronal Ca^{2+} homeostasis, which manifests as a secondary, delayed and irreversible [Ca^{2+}]$_c$ increase in the supramicromolar range, eventually leading to cell death (17). We used fura-FF to detect glutamate toxicity by calculating the number of cultured neurons showing the characteristic secondary Ca^{2+} increase during sustained (up to 30 min) glutamate stimulation. The percentage of neuronal death after stimulation with 10 μM glutamate was reduced in *Surf1*^{loxP}−/− neurons as compared to *Surf1*+/+ neurons, and it remained significantly lower at 100 μM glutamate stimulation (% cell death at 10μM glutamate: *Surf1*+/+17,1 ± 5,0% versus *Surf1*^{loxP}−/−6,7 ± 2,9%; at 100 μM glutamate *Surf1*+/+32,5 ± 5,0% versus *Surf1*^{loxP}−/− 16,9 ± 2,4% $P < 10^{-2}$; Fig. 6C).

Reduced mitochondrial Ca^{2+} uptake is responsible for reduced Ca^{2+} influx in *Surf1*^{loxP}−/− neurons

The extent of mitochondrial Ca^{2+} uptake, strategically located at plasma membrane Ca^{2+} entry sites, has been shown to regulate Ca^{2+} influx through different plasma membrane channels, such as capacitative or ligand-induced Ca^{2+} influx channels (17). Ca^{2+} buffering in the sub-plasma membrane space was shown to reduce Ca^{2+} feedback inhibition of capacitative Ca^{2+} influx channels as well as of diverse subunits of NMDA channels (18,19). In order to verify that the reduction of [Ca^{2+}]$_c$ following glutamate stimulation in *Surf1*^{loxP}−/− neurons was correlated to a modification of mitochondrial Ca^{2+} homeostasis, determining reduced Ca^{2+} influx, we measured mitochondrial [Ca^{2+}] ([Ca^{2+}]$_m$) in intact and permeabilized neurons, using a mitochondrially targeted low affinity aequorin probe (*mitAEQmut*). Neurons were transfected with the *mitAEQmut* probe and [Ca^{2+}]$_m$ was measured in *Surf1*+/+ and *Surf1*^{loxP}−/− cell populations after stimulation with glutamate at low (10 μM) and high (100 μM) concentrations. Stimulation with 100 μM glutamate induced very high increase of [Ca^{2+}]$_m$, leading to immediate consumption of the probe. However, mitochondrial Ca^{2+} transients could be measured at a lower dose of glutamate (10 μM). In these conditions (Fig. 7A), the mitochondrial Ca^{2+} uptake was drastically reduced in *Surf1*^{loxP}−/− versus *Surf1*+/+ cells. Maximum [Ca^{2+}]$_m$ was 28.95 ± 2.50 mM in *Surf1*^{loxP}−/− neurons ($n = 24$) versus 50.95 ± 3.36 mM in *Surf1*+/+ neurons ($n = 21$), $P < 10^{-5}$.

In order to verify that the reduction of mitochondrial Ca^{2+} uptake in *Surf1*^{loxP}−/− cells is due to lack of Surf1p, rather than to reduced cytosolic Ca^{2+} response consequent to reduced Ca^{2+} influx through the plasma membrane, neurons expressing the *mitAEQmut* probe were treated with low-dose digitonin, which selectively permeabilizes the plasma membrane, and endogenous cytosolic Ca^{2+} was washed out by perfusion with Ca^{2+}-free intracellular buffer. Mitochondrial Ca^{2+} uptake was then triggered by the addition of 1 μM

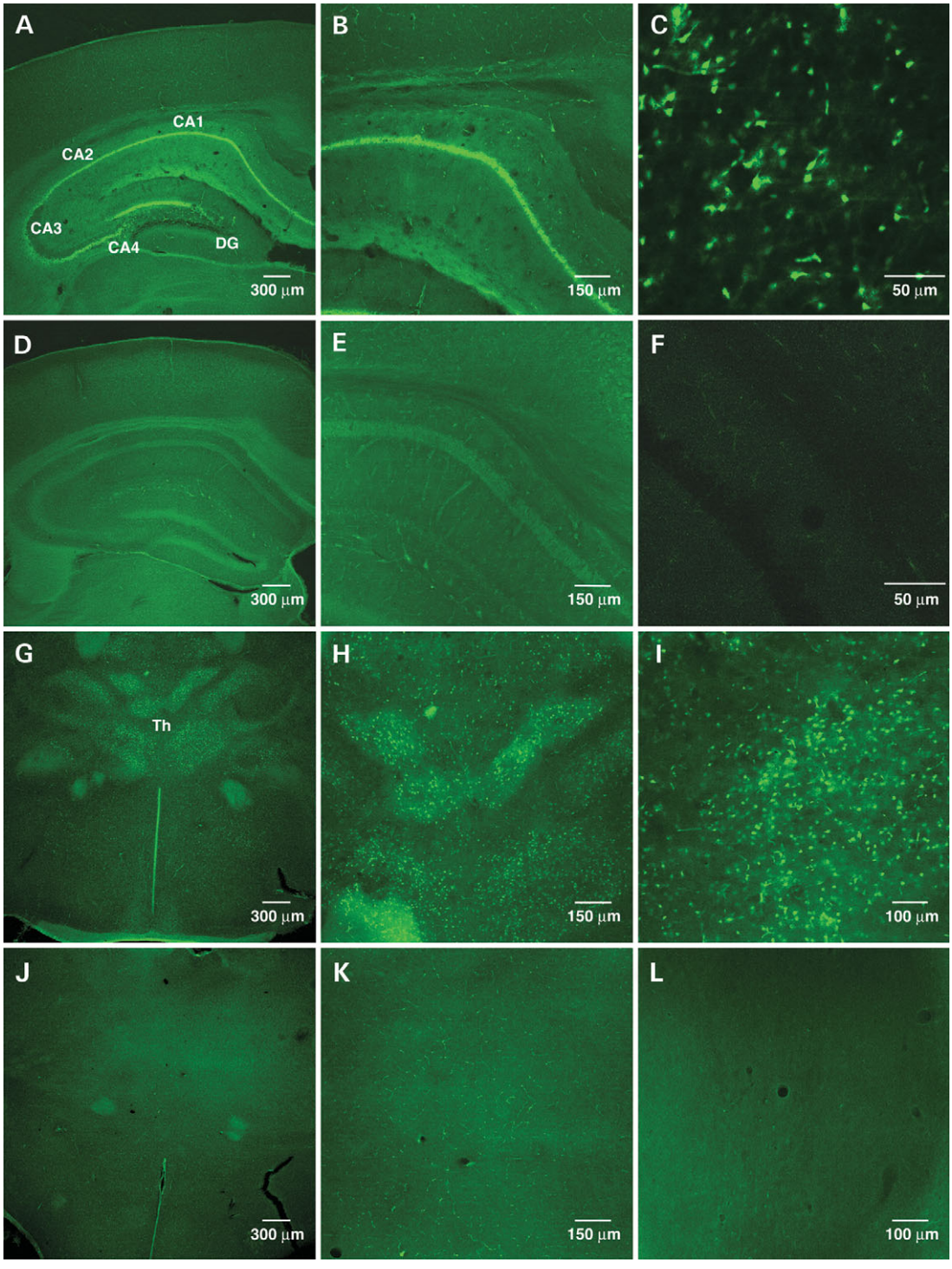

Figure 4. Low, medium and high magnifications of FJB-stained brain coronal sections, taken 2 days after kainate-induced level-5 seizures. (**A–C**) *Surf1* +/+ hippocampus; (**D–F**) *Surf1*^{loxP}−/− hippocampus; (**G–I**) *Surf1*+/+ thalamic nuclei; (**J–L**) *Surf1*^{loxP} −/− thalamic nuclei.

Ca^{2+} to the buffer. Again, the velocity of mitochondrial Ca^{2+} uptake was drastically reduced in *Surf1*^{loxP}−/− cells (*Surf1*^{loxP}−/− 0.34 ± 0.07 μM/s $n = 23$ versus *Surf1*+/+ 1.10 ± 0.12 μM/s $n = 26$, $P < 10^{-7}$) (Fig. 7B). This result indicates that the reduction of mitochondrial Ca^{2+} uptake is intrinsic to *Surf1*^{loxP}−/− mitochondria. Since the inhibition of mitochondrial Ca^{2+} uptake has been shown to augment the feedback inhibition of plasma-membrane Ca^{2+} channels in neurons, the impairment of mitochondrial Ca^{2+} buffering in *Surf1*^{loxP}−/− neurons might ultimately prevent them from Ca^{2+} overload, which could explain their refractoriness to DCD and cell death.

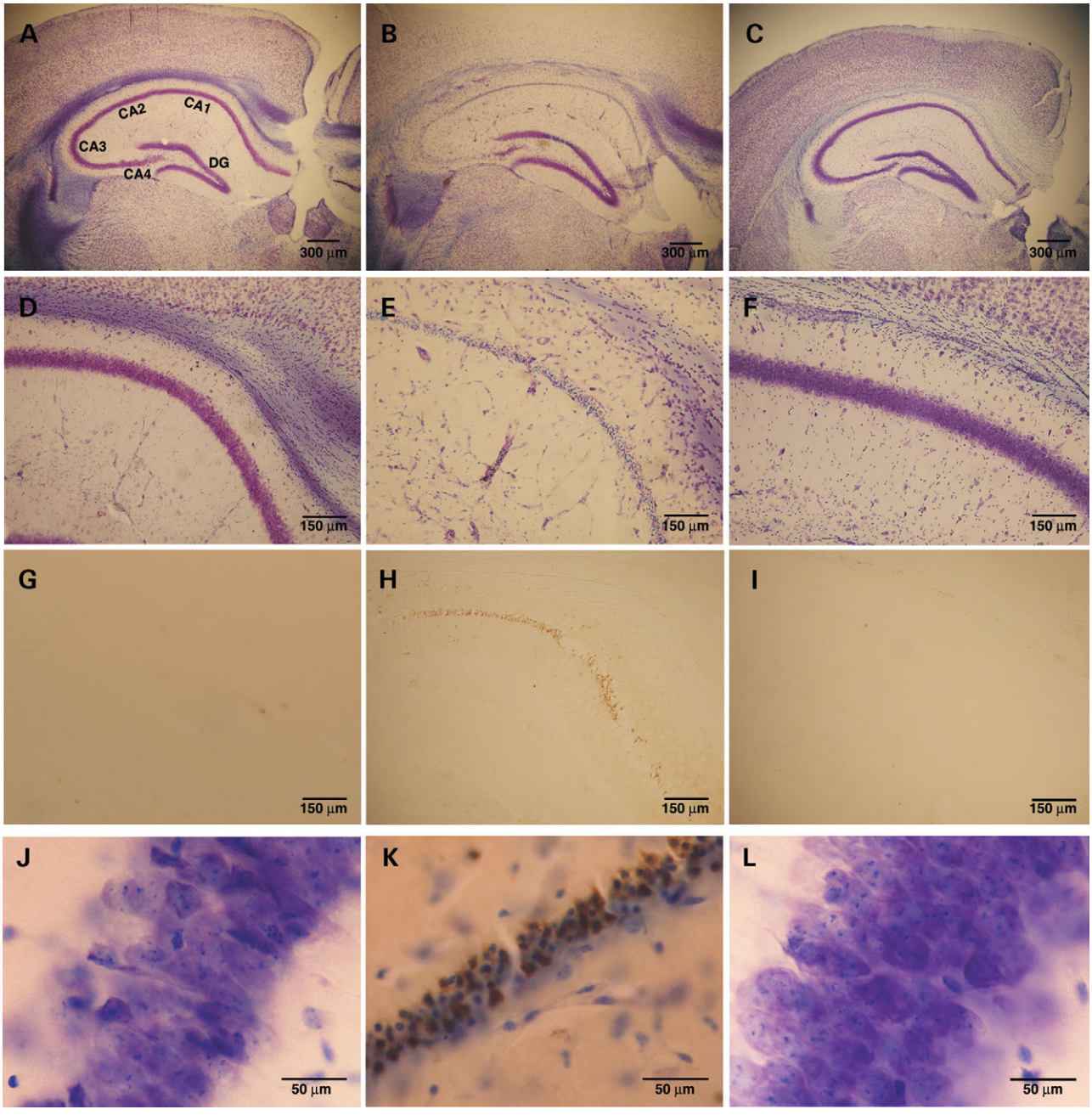

Figure 5. Low (**A**–**C**) and high (**D**–**F**) magnifications of brain coronal sections taken 2 days after kainate-induced level-5 seizures. Thionine staining in a treated *Surf1*+/+ brain shows massive loss of hippocampal CA neurons (B, E); the same area in a *Surf1*^{loxP}−/− brain (C, F) is comparable to an untreated control brain (A, D). The *gyrus dentatus* (DG) of hippocampus, which is adjacent to the CA area, but does not contain glutamatergic projections, is normal in all samples. TUNEL staining on CA1 in an untreated *Surf1*+/+ brain (**G**) a treated *Surf1*+/+ brain (**H**), in or in a treated *Surf1*^{loxP}−/− brain (**I**). Similar results are shown by high magnification of Thionine + TUNEL double stained CA3 neurons in an treated *Surf1*+/+ (**K**), untreated *Surf1* +/+ (**J**) and treated *Surf1*^{loxP}−/− (**L**).

Surf1 deficiency impairs mitochondrial Ca^{2+} uptake without changing the mitochondrial structure and membrane potential

The mitochondrial membrane potential ($\Delta\Psi_m$) drives the mitochondrial Ca^{2+} uptake by sustaining the activity of the mitochondrial Ca^{2+} uniporter (20,21). Therefore, reduction of $\Delta\Psi_m$ can decrease the driving force of Ca^{2+} entry and the activity of the Ca^{2+} uniporter machinery in the inner mitochondrial membrane, thus determining reduced Ca^{2+} uptake into the organelle. Since Surf1p plays a role in the formation of COX, and the latter is in turn involved in the maintenance of mitochondrial transmembrane H^+ gradient and $\Delta\Psi_m$, the reduction of Ca^{2+} uptake observed in *Surf1*^{loxP}−/− neurons could depend on a reduction of $\Delta\Psi_m$. We then measured the $\Delta\Psi_m$ in *Surf1*+/+ and *Surf1*^{loxP}−/− neuronal populations

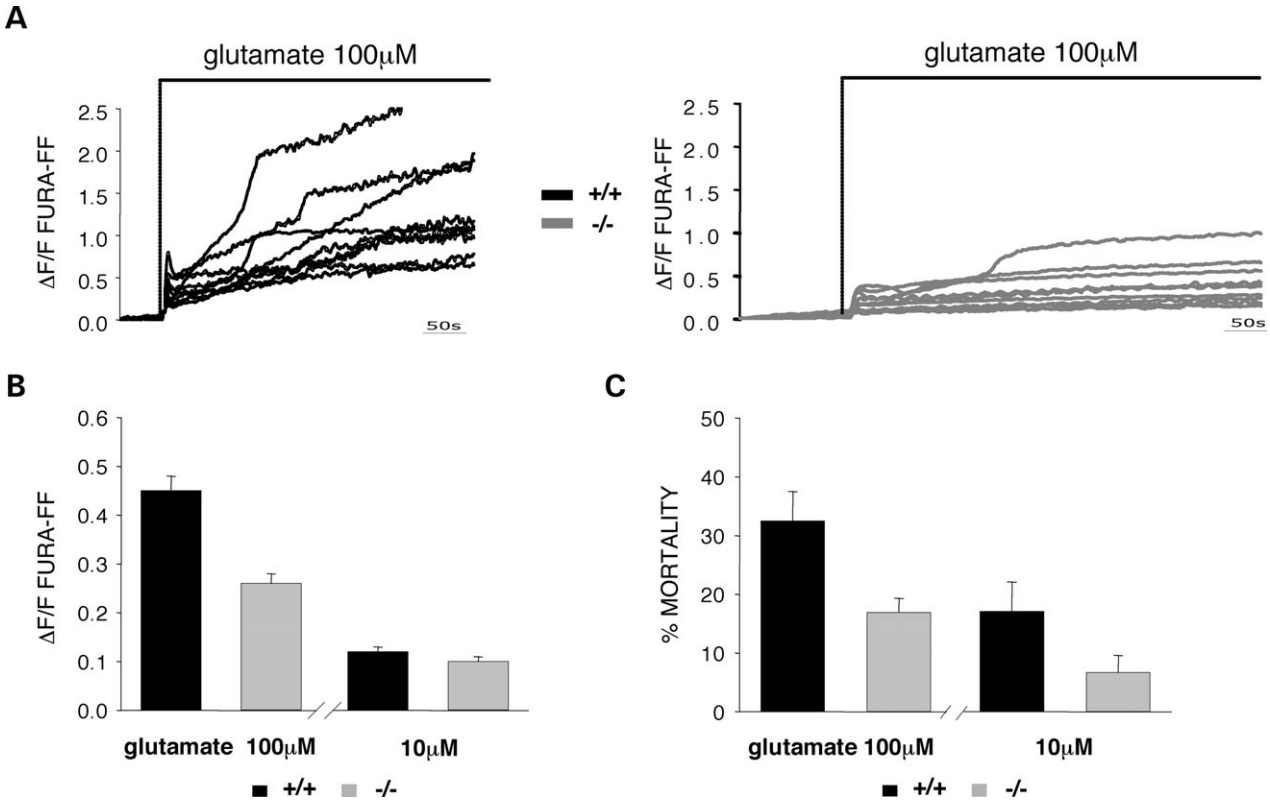

Figure 6. Cytosolic Ca^{2+} response of primary cultured *Surf1* + /+ and *Surf1*^{loxP}−/− neurons to glutamate measured by fura-FF. Values are expressed in relative change of 340/380 nm excitation ratio (⊗ F/F). (**A**) $[Ca^{2+}]_c$ response shows a biphasic elevation to glutamate challenge: the immediate increase is due to NMDA channel activation, whereas the secondary delayed increase is the result of delayed cellular Ca^{2+} deregulation. (**B**) Means ± SEM values of the primary peak response. (**C**) Percentage of cells undergoing Ca^{2+} deregulation from the total imaged cell population were calculated as an index of excitotoxic neuronal cell death.

by steady-state loading of neurons with the $\Delta\Psi_m$-sensitive dye teramethyl-rhodamine-methylester (TMRM), followed by fluorimetric measurement of the intensity of the dye in mitochondria. Our results showed no difference in the steady-state distribution of TMRM in *Surf1*^{loxP}−/− versus *Surf1*+/+ neurons (31.19 ± 0.23 in *Surf1*+/+ versus 32.12 ± 0.29 in *Surf1*^{loxP}−/−, fluorescence intensity in arbitrary units, Fig. 8A), demonstrating that the mild reduction observed in COX activity in various tissues of Surf1^{loxP}−/− animals failed to result in significant changes of $\Delta\Psi_m$.

We previously showed that mitochondrial fragmentation in epithelial cells leads to an average reduction of mitochondrial Ca^{2+} load upon IP_3-induced Ca^{2+} release (22). Therefore, we next investigated whether Surf1 deficiency can change the shape of the mitochondrial network. Neurons were transfected with mitochondrially targeted DsRed probe (*mtDsRed*) and the structure of mitochondria in 300 *Surf1*^{loxP}−/− and 300 *Surf1* + /+ individual cells was imaged by digital microscopy (22). As exemplified in Fig. 8B, the overall arrangement of the mitochondrial network did not appear to be disturbed in *Surf1*^{loxP}−/− neurons with respect to controls.

On the basis of these results, we concluded that Surf1p deficiency in mice does not lead to reduced $\Delta\Psi_m$ or altered mitochondrial structure, suggesting that the effect of Surf1p on mitochondrial Ca^{2+} uptake could be independent from its role on COX assembly and maintenance of $\Delta\Psi_m$.

To further confirm this hypothesis, we analyzed the effects of *SURF1* overexpression on global cellular and mitochondrial Ca^{2+} signals in HeLa cells. HeLa cells were co-transfected with a vector expressing human *SURF1* (*hSURF1*) (6) and with *mitAEQmut* or its non-targeted cytosolic variant (*cytAEQ*). Cells were then challenged with histamine (100 μM), which induces IP_3-dependent Ca^{2+} release from the ER. The resulting rise in $[Ca^{2+}]_c$ stimulates the mitochondrial Ca^{2+} uptake at sites located in proximity of the ER Ca^{2+} release sites. As shown on Figure 8C, the cytosolic Ca^{2+} responses remained unaltered in cells overexpressing *SURF1* (peak $[Ca^{2+}]_c$ 3.06 ± 0.08 mM in controls versus 2.86 ± 0.09 mM in *hSURF1* overexpressing cells); however, mitochondrial Ca^{2+} uptake was significantly increased by *SURF1* overexpression (peak $[Ca^{2+}]_m$ 78.07 ± 5.32 mM in controls versus 94.51 ± 6.04 mM in overexpressing cells, $P < 0.05$, Fig. 8D). This increase was not due to variations of the $\Delta\Psi_m$, as measured by TMRM uptake (data not shown).

DISCUSSION

High embryonic lethality was a major feature of a mouse *knockout* model for Surf1p, an accessory assembly factor of COX, based on the replacement of a region of several kb in

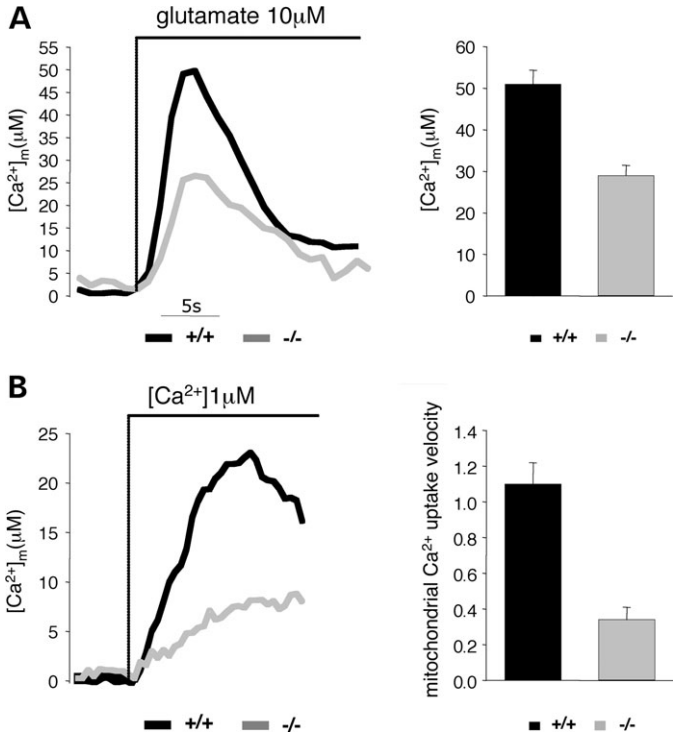

Figure 7. Mitochondrial Ca^{2+} uptake of primary cultured *Surf1* +/+ and *Surf1*^{loxP} −/− neurons measured by the recombinant low affinity *mitAEQmut* probe targeted to mitochondria. (**A**) Representative traces of luminescent values converted to $[Ca^{2+}]$ (41) are shown on the left panel; mean ± SEM of $[Ca^{2+}]_m$ peaks are shown on the right panel. (**B**) The same experiment as in A was carried out on cells treated with 25 μM digitonin for 1 min. Representative traces of $[Ca^{2+}]_m$ values are shown on the left panel; mean ± SEM of Ca^{2+} uptake velocity (micromol/s) are shown on the right panel.

the midportion of the *Surf1* gene with a *NEO* cassette (*Surf1*^{NEO}). The new mouse model reported here carries a recombinant *null* allele, consisting in the insertion of the 35 bp *loxP* sequence within exon 7 of the murine *Surf1* gene (*Surf1*^{loxP}). The restoration of mendelian distribution of the genotypes in newborn recombinant *Surf1*^{loxP} mice indicates that the embryonic lethality observed in the previous *Surf1*^{NEO} model was not a consequence of the ablation of the *Surf1* gene itself, but was rather due to the presence of the *NEO* cassette or to the elimination of regulatory elements contained in the deleted region of the *Surf1* gene. This conclusion is further supported by the observation that the *Surf1*$^{loxP\text{-}NEO\text{-}loxP}$ allele, from which the *Surf1*^{loxP} allele is derived, was again associated with 100% embryonic lethality, when present in homozygosity. Several recent reports (reviewed in 23) have shown that the maintenance of a *NEO* cassette in recombinant alleles can be associated with a number of unpredictable effects, including the creation of hypomorphic alleles, altered gene expression and embryonic lethality, mostly due to the promotion of illegitimate splicing of either the targeted gene or neighboring genes. The latter phenomenon was likely to occur in the *surfeit* genomic region, which is packed with six housekeeping genes, some of which share common regulatory elements (24).

Although SURF1p is a ubiquitously expressed mitochondrial protein, and its ablation leads to an early onset, invariably fatal encephalopathy in humans, no clinical disease phenotype could be observed in our *Surf1*^{loxP}−/− mice at any age. This situation is similar to that reported for the *Surf1*^{NEO}−/− animals that survived embryonic selection (11). The absence of neurological and extra-neurological abnormalities was associated with a biochemical phenotype that showed a specific and generalized defect of COX activity, however less severe than that observed in *SURF1* mutant patients (7). The COX defect was likely too mild to cause brain failure or impairment, but was possibly sufficient to determine the modest functional and morphological alterations found in skeletal muscle of adult *Surf1*^{loxP}−/− mice.

The mild biochemical and the virtually absent clinical phenotypes of *Surf1*^{loxP}−/− mice suggest that, in spite of the ubiquitous expression and high evolutionary conservation of Surf1p, the function of this protein in COX assembly is either ancillary or redundant, that is, it can partly be overtaken by other unknown factors. To some extent, this may well be true also in *SURF1*-less mutant patients, in whom fully assembled COX is diminished, but not absent (6). The different severity of the phenotype associated with the absence of Surf1p may then depend on the efficiency and efficacy of compensatory genetic or epigenetic mechanisms acting in different organisms, notably fungi, mice and men.

In an attempt to determine whether the reduced COX activity found in *Surf1*^{loxP}−/− animals could make their brain more sensitive to energy stress, we used an excitotoxic glutamate agonist, kainic acid, which triggers epileptic seizures in experimental animals. Kainic acid acts on the AMPA-kainate glutamate receptors present on the neuronal cell membrane (25). When activated, the Na^+-channel component of these receptors opens up, thus determining Na^+ influx and membrane depolarization. As a consequence, massive influx of Ca^{2+} occurs through the NMDA receptors and the VOCC channels of the plasma membrane (26). In addition to determining the epileptic discharge, the marked rise of $[Ca^{2+}]_c$ can promote a cascade of secondary effects that may ultimately lead to cell death (27).

These experiments were aimed at challenging the OXPHOS reserve of neuronal cells provoked by epileptic discharge. The same approach has been used in the recent past to precipitate catastrophic neurodegeneration in the MItochondrial Late-Onset Neurodegeneration (MILON) mouse, a conditional TFAM *knockout* model, characterized by loss of mtDNA in neurons of the frontal cortex (28). To our surprise, however, the elicitation of level-5 seizures failed to cause any neuronal degeneration and neuronal loss in *Surf1*^{loxP}−/− mice, while these lesions were consistently observed in glutamatergic areas of control brains. Since kainate-associated neurodegeneration is largely dependent on perturbation of Ca^{2+} homeostasis, we investigated the cytosolic and mitochondrial Ca^{2+} fluxes in primary neuronal cell cultures from *Surf1*^{loxP}−/− and control mice. The results of these experiments can be summarized as follows.

First, the ablation of *Surf1* drastically reduces the glutamate-induced increase of $[Ca^{2+}]$ in both cytosolic and mitochondrial compartments.

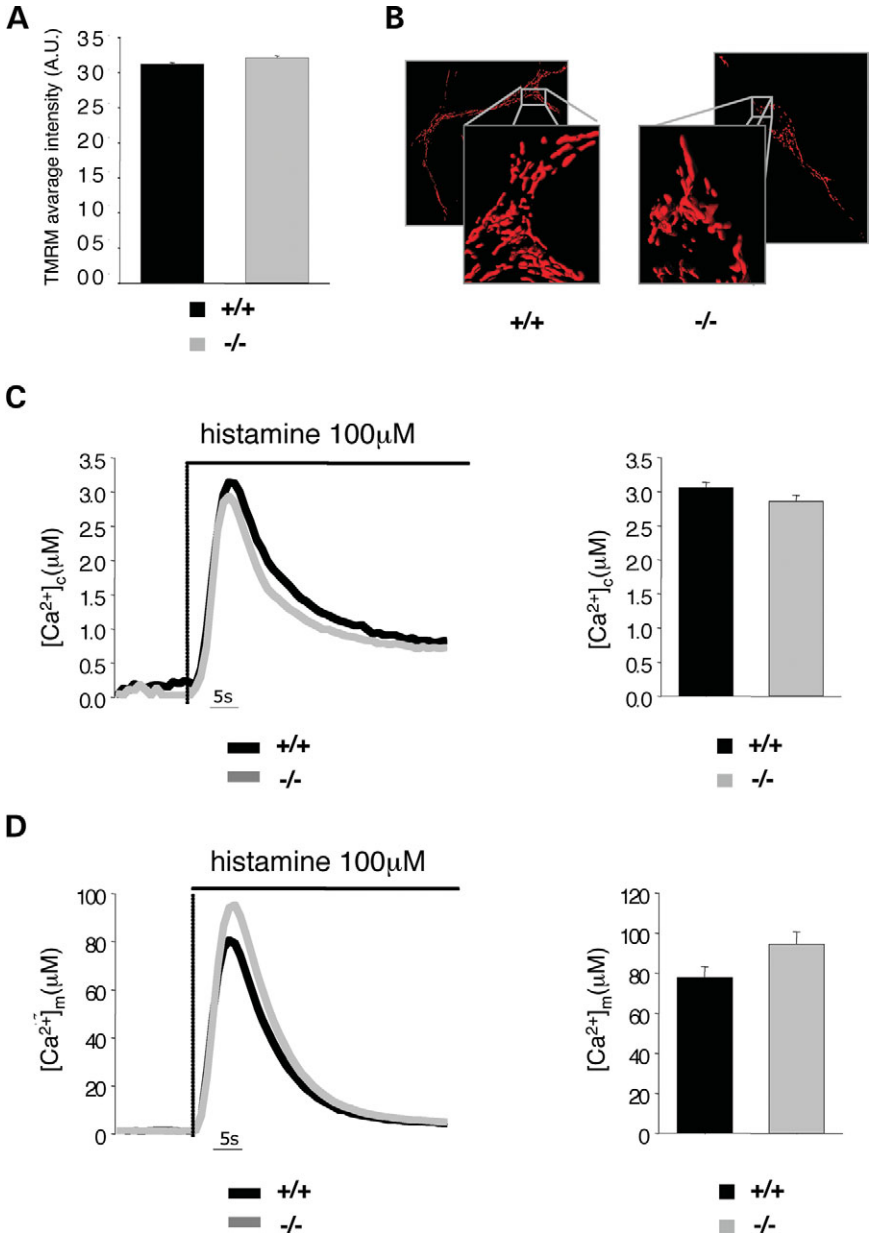

Figure 8. (**A**) Mitochondrial membrane potential is unchanged between *Surf1*$^{loxP}-/-$ and +/+ neuronal cells. A.U., arbitrary units. (**B**) Mitochondrial structure remains unchanged in *Surf1*$^{loxP}-/-$ neurons. Representative images of whole neurons and somata (zoomed insets) are shown. (**C** and **D**) Analysis of cytosolic (C) and mitochondrial (D) Ca^{2+} homeostasis in HeLa cells overexpressing *hSURF1* protein. Representative traces are shown on the left panels. Right panels show the mean ± SEM peak values after histamine stimulation from >10 experiments.

Second, the reduction of mitochondrial Ca^{2+} uptake is directly consequent to the absence of Surf1p.

Third, *Surf1*$^{loxP}-/-$ cultured neurons are much more resistant to glutamate toxicity than control neurons. How could this effect be linked to the observed reduction of mitochondrial Ca^{2+} uptake? One possibility is that reduced buffering capacity by *Surf1*$^{loxP}-/-$ mitochondria can determine the saturation of the Ca^{2+} microdomains in the contact sites between mitochondria and the plasma membrane or the ER. This effect could in turn promote the feedback closure of the Ca^{2+} channels in the above structures, thus inhibiting the $[Ca^{2+}]_c$ transient rise (18). Although speculative, this hypothesis can offer a mechanistic explanation for the neuroprotection observed *in vivo*. A second possibility is that the ablation of Surf1 may alter the expression of nuclear genes encoding proteins engaged in Ca^{2+} homeostasis. As a preliminary result, quantitative PCR analysis failed to show different expression of the Ca^{2+}–Na^{+} plasma membrane exchanger (NCX1) in *Surf1*$^{loxP}-/-$ versus *wt* brains (data not shown). More work is needed to expand this analysis to other Ca^{2+}-related genes.

Fourth and last, the reduction of the mitochondrial $[Ca^{2+}]$ uptake seems not to be dependent from a decrease of the $\Delta\Psi_m$, as a consequence of partial defect of COX activity

and mitochondrial respiration. This conclusion, which was also supported by the results of *hSURF1* overexpression in HeLa cells, suggests that Surf1p could play a direct role on mitochondrial Ca^{2+} handling, partially or completely independent from its function as a COX assembly factor. More work is necessary to test this hypothesis, but it is interesting to observe that an increasing number of mitochondrial proteins have been established to carry out multiple functions. A well known example is cytochrome c, which acts as both a redox electron shuttle of the MRC, and as an apoptogenic messenger (29). Likewise, the apoptosis-inducing factor (AIF), a flavoprotein closely associated with the mitochondrial inner membrane, has been implicated as both a cell death-promoting molecule and a regulator of activity and protein expression of MRC complex I (30). Lastly, $p66^{Shc}$ is an electron-transfer redox enzyme of the mitochondrial intermembrane space, which controls the production of reactive oxygen species (ROS), and regulates Ca^{2+} transport by acting on plasmamembrane Ca^{2+}-ATPases. These two independent activities can ultimately converge and synergize in mediating $p66^{Shc}$-dependent apoptosis (31). Targeted disruption of $p66^{Shc}$ is associated with prolonged lifespan in mice, possibly related to its role on the control of ROS production.

Similar to the $p66^{Shc}-/-$, our $Surf1^{loxP}-/-$ mouse model displays significantly increased longevity. Of note, increased longevity was also observed in a CNS-restricted conditional *Surf1 knockdown* (KD) model in *Drosophila melanogaster*, whereas the corresponding constitutive model was embryonic lethal (32). We do not have an explanation for this observation, which is in striking contrast with the early onset, invariably fatal phenotype associated with the loss of SURF1p function in humans. It is possible that the COX defect in $Surf1^{loxP}-/-$ mice is not severe enough to confer selective disadvantage in a 'protected' environment such as an animal care facility. These data are nevertheless surprising, considering that COX deficiency associated with Surf1p disruption should in principle determine an increase of ROS (33), which are proposed to play a major role in the aging process (34). An attractive possibility is that the effect on longevity is due to the role of Surf1p on mitochondrial Ca^{2+} uptake and cellular Ca^{2+} homeostasis. This effect is likely to be hidden in organisms, such as *S. cerevisiae* and *Homo sapiens*, in which lack of Surf1p leads to severe impairment of COX assembly and faulty OXPHOS, whereas it would be unmasked in other organisms, such as *Mus musculus* and the conditional *D. melanogaster* KD model, characterized by less severe impairment of COX assembly and OXPHOS phenotype.

MATERIALS AND METHODS

Creation of $Surf1^{loxP\text{-}NEO\text{-}loxp}+/-$ and $Surf1^{loxP}-/-$ recombinant mice

The list of all primers is provided in the Supplementary Material, Table 2.

For the construction of the *Surf1* recombinant alleles, we used a 10 kb *Hind*III-*Eco*RI fragment containing the entire *Surf1* and *Surf2* genes, and part of *Surf4* and *Surf3* genes, cloned in BlueScript SK. A fragment of approximately 1.2 kb, composed of the gene encoding the neomycin phosphotransferase (*NEO* cassette) flanked by two 35-mer identical *loxP* sites (*loxP-NEO-loxP*), was inserted in the unique *Acc*III site contained in exon 7 of the *Surf1* murine gene corresponding to nt 670 of the *Surf1* cDNA. The DNA vector was verified on both strands by automated sequence analysis using the big-dye terminator kit and protocol (Applied Biosystems), on a 3100 ABI apparatus.

Gene targeting by electroporation of the *Hind*III-linearized vector into AB1 ES cells, derived from 129/SvEvBr ♀≠/Hprt-bm2 mouse substrain (a kind gift from Alan Bradley), and generation of chimeras, were performed as described (35). Three hundred colonies that survived selection with the neomycin analogue drug G-418 (200 μg/ml) were screened for homologous recombination by PCR and Southern blot analyses.

For diagnostic PCR analysis, a 2 kb DNA fragment was amplified using a forward primer corresponding to a region inside the NEO cassette and a reverse primer corresponding to a sequence within the *Surf3* gene located outside the recombinant region. For diagnostic Southern blot analysis (Fig. 1B) on the 5′ end of the recombinant region, 10 μg of ES genomic DNA was digested with *Eco*RI, run through a 0.8% agarose gel in 1X TE buffer, blotted on a nitrocellulose filter and hybridized with a 0.7 kb PCR fragment (probe P1 in Fig. 1) radiolabeled with [α^{32}P]-dCTP (NEN, Boston, MA, USA) using the 'Ready-to-go' random priming kit (Amersham, Piscataway, NJ, USA). P1 corresponds to a region of the *Surf5* gene outside but contiguous to the recombinant region. The *wt Surf1* allele corresponds to a 19 kb hybridization band, whereas the $Surf1^{loxP\text{-}NEO\text{-}loxP}$ recombinant allele corresponds to 13 and 7 kb bands due to the presence of an *Eco*RI site within the *NEO* cassette. For diagnostic Southern blot analysis on the 3′ end, DNA was digested with *EagI* and *HindIII*, separated by electrophoresis and blotted as above. Hybridization was then carried using a 0.8 fragment corresponding to a sequence on the *Surf4* gene outside but contiguous to the recombinant region (probe P2 in Fig. 1). The *wt* allele corresponds to a hybridization band of 9.2 kb, whereas the $Surf1^{loxP\text{-}NEO\text{-}loxP}$ recombinant allele corresponds to a band of 7.5 kb, again due to the presence of an extra *Eag*I site within the *NEO* cassette.

Two of the five ES clones that showed homologous recombination were injected in B6D2F1♀ ≠ C57/Bl6J blastocysts (36). Chimeric pups were identified by the presence of agouti hair and, on maturity, mated with B6D2F1 (C57/Bl6J_DBA2) females to check for the contribution of the ES cells to the germline.

For the creation of $Surf1^{loxP}$ animals, $Surf1^{loxP\text{-}NEO\text{-}loxP}+/-$ mice of mixed BDF1 genetic background were mated to *cre* mice. Compound heterozygotes ($Surf1^{loxP/+;cre/+}$) were identified by PCR and backcrossed to each other.

For genotyping, 250 ng genomic DNA extracted from tail tips was PCR amplified in 50 μl of 1 × $MgCl_2$-PCR *buffer* (Applied Biosystems), 200 μM dNTPs, 0.6 μM each dNTPs and 0.03 U/μl *Taq* Polymerase (Applied Biosystems), 5% DMSO. After an initial denaturation at 94°C for 2 min, each of the 35 PCR cycles was as follows: 94°C for 30 s, 58°C for 60 s, 72°C for 90 s. Final extension was at 72°C for 5 min. For the $Surf1^{loxP\text{-}NEO\text{-}loxP}$ allele, we used a single

forward primer (LNL-FW) and two distinct reverse primers, one internal to the *NEO* cassette (LNL-RV1) specific to the recombinant allele, and another corresponding to a *Surf1* region (LNL-RV2) specific to the *wt* allele. The recombinant allele generates a PCR fragment of 583 bp, whereas the *wt* allele generates a PCR fragment of 458 bp. For the *Surf1*^{loxP} allele, we used the forward primer LP-FW, corresponding to a region of *Surf1* exon 6; and the reverse primer LP-RV, corresponding to a region of *Surf1* exon 7. The PCR produces a 305 bp *wt* DNA fragment and a 340 bp recombinant fragment). The *cre* transgene was detected by using the forward primers CRE-FW and the reverse primer CRE-RV (PCR fragment 590 bp).

Animal studies were approved by the animal welfare Ethics Committee of the National Neurological Institute in accordance with the Institutional Animal Care and Use Committee guidelines. Standard food and water were given *ad libitum*.

RT-PCR analysis

To evaluate the presence of recombinant *Surf1*^{loxP} transcript, total RNA was extracted from brain, liver, muscle and heart of four *Surf1*$^{loxP}-/-$ and four *Surf1* +/+ adult animals, using the RNeasy lipid tissue kit (QIAGEN Sciences, MD, USA) following the manufacturer's protocol. Total RNA was used as a template for reverse transcription, using the 'cDNA cycle' kit and protocol (Invitrogen, Carlsbad, CA, USA). Total cDNA was purified and resuspended in a final volume of 20 μl and used for PCR amplification of individual cDNA fragments corresponding to *GAPDH* and *Surf1* genes; 3 μl were then used in each 50 μl PCR reaction containing 1 × $MgCl_2$-PCR buffer, 200 μM dNTPs, 5% DMSO, 0.6 μM of each primer and 0.03 U/μl of *Taq*-Gold polymerase (Invitrogen, Carlsbad, CA, USA). *GAPDH* was detected using primers GAPDH-FW and GAPDH-RV. The *wt* and *Surf1*^{loxP} transcripts were PCR-diagnosed using exonic primers LP-FW and LP-RV (Fig. 1E).

Western blot analysis

Western blot analysis was performed on electroblotted denaturing sodium-dodecyl sulphate polyacrylamide gel electrophoresis (SDS–PAGE), and two-dimension blue native electrophoresis (2D-BNE), as described previously (6). Approximately 100 μg non-collagenous protein was used for each sample in SDS-PAGE and 20 μg of isolated mitochondria in 2D-BNE. Chemiluminescence-based immunostaining (ECL kit, Amersham) was performed using the following antibodies: polyclonal antibody AS182–196 (6) raised against amino acid sequence 82–96 of mouse Surf1p, which is at the N-terminal of the truncated protein predicted by the *Surf1*^{loxP} allele; monoclonal antibodies against subunits COX I and COX IV (Molecular Probes, Eugene, OR, USA) and Surf1p (Mitosciences LLC, Eugene, OR, USA).

Morphological analysis

For light microscopy, samples from different organs were frozen in liquid-nitrogen-cooled isopentane. Standard histological and histochemical techniques for the detection of mitochondrial alterations and muscle fiber distribution were performed on serial cryostat cross sections as previously described (37).

Biochemical analysis

Biochemical assays of individual respiratory complexes were carried out on tissue homogenates (38). Specific activities of each complex were normalized to that of CS, an indicator of the number of mitochondria. Blood lactate was measured using the 'Lactate reagent' kit and protocol (Sigma, St Louis, MO, USA).

Rotarod test

Motor performance tests were given to 13 *wt* mice and to 13 *Surf1*$^{loxP}-/-$ mice. All animals were 3 months old. The rotating rod test was performed on a Rotarod apparatus for mice (Ugo Basile) (39).

Kainate-induced seizures and brain analysis

Kainic acid was dissolved in isotonic saline (pH 7) with a drop of 1 M NaOH and administered *i.p.* Mice were monitored continuously for at least 3 h after injection to determine the onset and level of seizures according to Sperk *et al.*, (13). For histological analysis of the brain, animals were treated with a lethal injection of 4% chloral hydrate before intracardiac perfusion with 4% paraformaldehyde in PBS. Brains were rapidly dissected and post-fixed overnight in the same solution. Serial rostro-caudal, 50 μm thick coronal brain sections were obtained using a Vibratome (Leica) and collected in 0.1 M PB at pH 7.2 with 0.01% NaN_3. One every 12 sections was labeled with FJB (Histo-Chem, Jefferson, AR) according to manufacturer's instructions. Adjacent sections were stained with 0.1% thionine. Next adjacent sections were labeled by *terminal deoxynucleotidyl transferase-mediated biotinylated UTP nick end labeling* (TUNEL) (Apoptag *in situ* Apoptosis Detection kit; Intergen, Purchase, NY) according to the manufacturer's instructions. Fluorescent images were acquired on a confocal microscope (Radiance 2100 confocal microscope, Bio-Rad, Hercules, CA, USA) using an FITC filter and optical photographs were acquired using a Nikon Eclipse E400 microscope and a Nikon DS-U1 digital camera.

Cortical/hippocampal primary neuronal cell cultures

Cortical/hippocampal neurons were prepared from 1- to 3-day-old newborn mice, according to Pasti *et al.* (40), and neurons were resuspended in NeurobasalA Medium (Gibco) with supplement B-27 (Gibco), GlutaMax (Gibco) and penicilline/streptomycine (Gibco) rigorously at 37°C and plated onto glass coverslips, coated with poly-D-lysine (Sigma).

Dynamic *in vivo* [Ca^{2+}] measurements with targeted aequorin probes

The construction and use of luminescent Ca^{2+} sensitive aequorin probes were previously described (41). All

aequorin measurements were carried out in KRB containing 1 mM $CaCl_2$ (KRB/Ca^{2+}, Krebs-Ringer modified Buffer: 135 mM NaCl, 5 mM KCl, 1 mM $MgSO_4$, 0.4 mM K_2HPO_4, 1 mM $CaCl_2$, 15 mM glucose, 20 mM HEPES, pH 7.4). For HeLa cells KRB contained 5 mM glucose. Experiments in permeabilized neurons were performed as previously described for HeLa cells (42), except that 25 μM digitonin was used, in order to preserve mitochondrial integrity.

Imaging procedures

Cortical cultures were loaded for 20 min with 3 μM fura-2FF/AM (or fura-2) (Teflabs, Austin, TX, USA) at 37°C in the cell culture medium (K_d of fura-2FF or fura-2 for Ca^{2+} is 5 and 55 μM, respectively; 43). Images were acquired on an epifluorescence inverted microscope Axiovert 200 (Zeiss, Germany) equipped with a 40× fluorite objective. $[Ca^{2+}]_c$ was monitored in single cells using two excitation light wavelengths, at 340 nm and 380 nm (Sutter Instrument Co., CA, USA). Emitted fluorescence light was selected by a 505–530 nm filter. Images were acquired by CCD camera (Roper Scientific, USA). All imaging data were collected and analyzed using the Metafluor 6.1 software. For the visualization of the mitochondrial network, Z-series of images of neurons were 3D deconvolved and reconstructed using a custom-made software (44).

Statistical analysis

Two-tailed, unpaired, unequal variance Student's *t*-test was used for statistical analysis. Survival probability was calculated using the Kaplan–Meier and log-rank tests.

SUPPLEMENTARY MATERIAL

Supplementary Material is available at HMG Online.

ACKNOWLEDGEMENTS

The authors are grateful to Barbara Geehan for revising the manuscript. They are also grateful to Chiara Falcone for assistance on statistical analysis and Mike Fried for the generous gift of a plasmid containing the mouse *surfeit* gene cluster.

This study was supported by Fondazione Telethon, Italy (Grant no. GGP030039), Fondazione Pierfranco e Luisa Mariani, MITOCIRCLE and EUMITOCOMBAT network grants from the European Union Framework Program 6. The work of R.R. was supported by grants from Telethon, Italy, the Italian Association for Cancer Research (AIRC), the Italian University Ministry (PRIN, FIRB and local research grants), the Emilia-Romagna PRRIITT program, the Ferrara Objective 2 funds and the Italian Space Agency (ASI).

Conflict of Interest statement. None declared.

REFERENCES

1. Pecina, P., Gnaiger, E., Zeman, J., Pronicka, E. and Houstek, L. (2004) Decreased affinity for oxygen of cytochrome-*c* oxidase in Leigh syndrome caused by *SURF1* mutations. *Am. J. Physiol. Cell Physiol.*, **287**, 1384–1388.
2. DiMauro, S., Zeviani, M., Rizzuto, R., Lombes, A., Nakase, H., Bonilla, E., Miranda, A. and Schon, E. (1988) Molecular defects in cytochrome c oxidase in mitochondrial diseases. *J. Bioenerg. Biomembr.*, **20**, 353–364.
3. Solans, A., Zambrano, A. and Barrientos, A. (2004) Cytochrome *c* oxidase deficiency: from yeast to human. *Preclinica*, **2**, 1–13.
4. Nijtmans, L.G., Taanman, J.W., Muijsers, A.O., Speijer, D. and Van den Bogert, C. (1998) Assembly of cytochrome-c oxidase in cultured human cells. *Eur. J. Biochem.*, **254**, 389–394.
5. Nijtmans, L.G., Artal Sanz, M., Bucko, M., Farhoud, M.H., Feenstra, M., Hakkaart, G.A., Zeviani, M. and Grivell, L.A. (2001) Shy1p occurs in a high molecular weight complex and is required for efficient assembly of cytochrome c oxidase in yeast. *FEBS Lett.*, **498**, 46–51.
6. Tiranti, V., Galimberti, C., Nijtmans, L., Bovolenta, S., Perini, M.P. and Zeviani, M. (1999) Characterization of SURF-1 expression and Surf-1p function in normal and disease conditions. *Hum. Mol. Genet.*, **8**, 2533–2540.
7. Munaro, M., Tiranti, V., Sandona, D., Lamantea, E., Uziel, G., Bisson, R. and Zeviani, M. (1997) A single cell complementation class is common to several cases of cytochrome c oxidase defective Leigh's syndrome. *Hum. Mol. Genet.*, **6**, 221–228.
8. Tiranti, V., Hoertnagel, K., Carrozzo, R., Galimberti, C., Munaro, M., Granatiero, M., Zelante, L., Gasparini, P., Marzella, R., Rocchi, M. *et al.* (1998) Mutations of SURF1 in Leigh disease associated with cytochrome c oxidase deficiency. *Am. J. Hum. Genet.*, **63**, 1609–1621.
9. Leigh, D. (1951) Subacute necrotizing encephalomyelopathy in an infant. *J. Neurol. Neurosurg. Psychiatry*, **14**, 216–221.
10. Duhig, T., Ruhrberg, C., Mor, O. and Fried, M. (1998) The human surfeit locus. *Genomics*, **52**, 72–78.
11. Agostino, A., Invernizzi, F., Tiveron, C., Fagiolari, G., Prelle, A., Lamantea, E., Giavazzi, A., Battaglia, G., Tatangelo, L., Tiranti, V. and Zeviani, M. (2003) Constitutive knockout of *Surf1* is associated with high embryonic lethality, mitochondrial disease and cytochrome c oxidase deficiency in mice. *Hum. Mol. Gen.*, **12**, 399–413.
12. Harkness, J.E. and Wagner, J.E. (1995) *The Biology and Medicine of Rabbits and Rodents*, 4th edn. Lea and Febiger, Philadelphia, PA.
13. Sperk, G., Lassmann, H., Baran, H., Seitelberger, F. and Hornykiewicz, O. (1985) Kainic acid-induced seizures: dose-relationship of behavioural, neurochemical and histopathological changes. *Brain Res.*, **338**, 289–295.
14. Schmued, L.C., Slikker, W., Jr. and Wang, G.J. (1998) Fluoro-Jade B: a bis homolog of Fluoro-Jade with improved degenerate neuron staining properties. *Soc. Neurosci. Ab.*, **24**, 1064.
15. Nicholls, D.G. and Budd, S.L. (2000) Mitochondria and neuronal survival. *Physiol. Rev.*, **80**, 315–360.
16. Duchen, M.R. (2000) Mitochondria and calcium: from cell signalling to cell death. *J. Physiol.*, **529**, 57–68.
17. Bano, D., Young, K.W., Guerin, C.J., Lefeuvre, R., Rothwell, N.J., Naldini, L., Rizzuto, R., Carafoli, E. and Nicotera, P. (2005) Cleavage of the plasma membrane Na^+/Ca^{2+} exchanger in excitotoxicity. *Cell*, **120**, 275–285.
18. Parekh, A.B. (2003) Store-operated Ca^{2+} entry: dynamic interplay between endoplasmic reticulum, mitochondria and plasma membrane. *J. Physiol.*, **547**, 333–348.
19. Sessoms-Sikes, S., Honse, Y., Lovinger, D.M. and Colbran, R.J. (2005) CaMKII-alpha enhances the desensitization of NR2B-containing NMDA receptors by an autophosphorylation-dependent mechanism. *Mol. Cell. Neurosci.*, **29**, 139–147.
20. Nicholls, D.G. (2005) Mitochondria and calcium signaling. *Cell Calcium*, **38**, 311–317.
21. Bernardi, P. (1999) Mitochondrial transport of cations: channels, exchangers, and permeability transition. *Physiol. Rev.*, **79**, 1127–1155.
22. Szabadkai, G., Simoni, A.M., Chami, M., Wieckowski, M.R., Youle, R.J. and Rizzuto, R. (2004) Drp-1-dependent division of the mitochondrial network blocks intraorganellar Ca^{2+} waves and protects against Ca^{2+}-mediated apoptosis. *Mol. Cell.*, **16**, 59–68.
23. Lewandoski, M. (2001) Conditional control of gene expression in the mouse. *Nature Reviews*, **2**, 743–755.

24. Huxley, C. and Fried, M. (1990) The mouse surfeit locus contains a cluster of six genes associated with four cpg-rich islands in 32 kilobases of genomic DNA. *Mol. Cell. Biol.*, **10**, 605–614.
25. Hunsberger, J.G., Bennett, A.H., Selvanayagam, E., Duman, R.S. and Newton, S.S. (2005) Gene profiling the response to kainic acid induced seizures. *Brain Res. Mol. Brain Res.*, **141**, 95–112.
26. Jaskolski, F., Coussen, F. and Mulle, C. (2005) Subcellular localization and trafficking of kainate receptors. *Trends Pharmacol. Sci.*, **26**, 20–26.
27. Zhu, X., Jin, S., Kong Ng, Y., Lee, W.L. and Wong, P.T.H. (2001) Positive and negative modulation by AMPA- and kainate-receptors of striatal kainate injection-induced neuronal loss in rat forebrain. *Brain Research*, **922**, 293–298.
28. Sorensen, L., Ekstrand, M., Silva, J.P., Lindqvist, E., Xu, B., Rustin, P., Olson, L. and Larsson, N.G. (2001) Late-onset corticohippocampal neurodepletion attributable to catastrophic failure of oxidative phosphorylation in MILON mice. *J. Neurosi.*, **21**, 8082–8090.
29. Garrido, C. and Kroemer, G. (2004) Life's smile, death's grin: vital functions of apoptosis-executing proteins. *Curr. Opin. Cell. Biol.*, **16**, 639–646.
30. Vahsen, N., Cande, C., Triere, J.J., Benit, P., Joza, N., Larochette, N., Mastroberardino, P.G., Pequignot, M.O., Casares, N., Lazar, V. *et al.* (2004) AIF deficiency compromises oxidative phosphorylation. *EMBO J.*, **23**, 4679–4689.
31. Giorgio, M., Migliaccio, E., Orsini, F., Paolucci, D., Moroni, M., Contursi, C., Pelliccia, G., Luzi, L., Minacci, S., Marcaccio, M. *et al.* (2005) Electron transfer between cytochrome c and p66Shc generates reactive oxygen species that trigger mitochondrial apoptosis. *Cell*, **122**, 221–233.
32. Zordan, M.A., Cisotto, P., Benna, C., Agostino, A., Rizzo, G., Piccin, A., Pegoraro, M., Sandrelli, F., Perini, G., Tognon, G. *et al.* (2006) Post-transcriptional silencing and functional characterization of the *Drosophila melanogaster* homolog of human Surf1. *Genetics*, **172**, 229–241.
33. Lee, I., Bender, E., Arnold, S. and Kadenbach, B. (2001) New control of mitochondrial membrane potential and ROS formation—a hypothesis. *Biol. Chem.*, **382**, 1629–1636.
34. Terman, A. and Brunk, U.T. (2006) Oxidative stress, accumulation of biological 'garbage', and aging. *Antioxid. Redox. Signal.*, **8**, 197–204.
35. Ramirez-Solis, R., Davis, A.C. and Bradley, A. (1993) Gene targeting in embryonic stem cells. *Meth. Enzymol.*, **225**, 855–878.
36. Bradley, A. (1987) Robertson, EJ (eds), *Production and Analysis of Chimaeric Mice in Teratocarcinomas and Embryonic Stem Cells, a Practical Approach.*, IRL Press, Oxford.
37. Sciacco, M. and Bonilla, E. (1996) Cytochemistry and immunocyto-chemistry of mitochondria in tissue sections. *Meth. Enzymol.*, **264**, 509–521.
38. Bugiani, M., Tiranti, V., Farina, L., Uziel, G. and Zeviani, M. (2005) Novel mutations in COX15 in a long surviving Leigh syndrome patient with cytochrome c oxidase deficiency. *J. Med. Genet.*, **42**, e28.
39. Dulioust, E., Toyama, K., Busnel, M.C., Moutier, R., Carlier, M., Marchaland, C., Ducot, B., Roubertoux, P. and Auroux, M. (1995) Long-term effects of embryo freezing in mice. *Proc. Natl Acad. Sci. USA*, **92**, 589–593.
40. Pasti, L., Pozzan, T. and Carmignoto, G. (1995) Long-lasting changes of calcium oscillations in astrocytes. A new form of glutamate-mediated plasticity. *J. Biol. Chem.*, **270**, 15203–15210.
41. Chiesa, A., Rapizzi, E., Tosello, V., Pinton, P., de Virgilio, M., Fogarty, K.E. and Rizzuto, R. (2001) Recombinant aequorin and green fluorescent protein as valuable tools in the study of cell signalling. *Biochem. J.*, **355**, 1–12.
42. Rapizzi, E., Pinton, P., Szabadkai, G., Wieckowski, M.R., Vandecasteele, G., Baird, G., Tuft, R.A., Fogarty, K.E. and Rizzuto, R. (2002) Recombinant expression of the voltage-dependent anion channel enhances the transfer of Ca^{2+} microdomains to mitochondria. *J. Cell Biol.*, **159**, 613–624.
43. Xu-Friedman, M.A. and Regehr, W.G. (1999) Presynaptic strontium dynamics and synaptic transmission. *Biophys. J.*, **76**, 2029–2042.
44. Rizzuto, R., Carrington, W. and Tuft, R.A. (1998) Digital imaging microscopy of living cells. *Trends Cell Biol.*, **8**, 288–292.